Proximally targeted GABAergic synapses and gap junctions synchronize cortical interneurons

Gábor Tamás[1,2], Eberhard H. Buhl[2,3], Andrea Lörincz[1,2] and Peter Somogyi[2]

[1] *Department of Comparative Physiology, University of Szeged, Középfasor 52, Szeged H-6726, Hungary*

[2] *MRC Anatomical Neuropharmacology Unit, University Department of Pharmacology, University of Oxford, Mansfield Road, Oxford, OX1 3TH, UK*

[3] *Present address: School of Biomedical Sciences, Worsley Building, University of Leeds, Leeds LS2 9NQ, UK*

Correspondence should be addressed to G.T. (gtamas@sol.cc.u-szeged.hu)

Networks of GABAergic interneurons are implicated in synchronizing cortical activity at gamma frequencies (30–70 Hz). Here we demonstrate that the combined electrical and GABAergic synaptic coupling of basket cells instantaneously entrained gamma-frequency postsynaptic firing in layers 2/3 of rat somatosensory cortex. This entrainment was mediated by rapid curtailment of gap junctional coupling potentials by $GABA_A$ receptor-mediated IPSPs. Electron microscopy revealed spatial proximity of gap junctions and GABAergic synapses on somata and dendrites. Electrical coupling alone entrained postsynaptic firing with a phase lag, whereas unitary GABAergic connections were ineffective in gamma-frequency phasing. These observations demonstrate precise spatiotemporal mechanisms underlying action potential timing in oscillating interneuronal networks.

Synchronous cortical population activity in the gamma frequency band (30–70 Hz) is seen in the electroencephalograms (EEGs) of humans and other mammals[1], and emerges from the concerted activity of many neurons. Gamma band EEG activity is associated with a number of cognitive processes, such as perception or attentional mechanisms[2–5]. Fast network oscillations are proposed to establish transient temporal correlations between spatially distributed neurons with a temporal resolution of less than ten milliseconds[6], and GABAergic mechanisms may be important in governing population activity[7–12]. Fast, synchronous firing of putative interneurons is recorded *in vivo*[13], and gamma rhythms arise as an emergent property of mutually connected networks of interneurons *in vitro*[14–16]. In addition to chemical transmission mechanisms, it is proposed that electrical coupling contributes to neuronal synchrony[17–19]. In fact, interneurons are connected via electrical synapses in several brain regions[20–22], and such electrical coupling can promote synchronous activity in differentially connected networks of cortical interneurons[21,22]. However, it is unknown whether interactions of axons and/or the somatodendritic domains of coupled cells mediate the electrical coupling in the cortex. Gap junctions, the anatomical substrate for electrical coupling, are reported between dendrites[23–25], as well as axons and soma/dendrites[26,27] in the central nervous system. A particular subcellular site of electrical communication might result in a highly localized, compartmental interaction of conductances, resulting in the domain specific processing of sub- and suprathreshold operations. Furthermore, chemical, GABA-mediated interactions are frequent between cortical interneurons[9,21,22,28,29], but the role of dynamic integration of GABAergic synaptic potentials with concurrent electrical coupling[21,22] in neural rhythmogenesis is largely unknown.

To identify the cellular mechanisms underlying interneuronal synchronization, we recorded pairs of interneurons coupled by chemical and/or electrical synapses in layers II/III of the rat somatosensory cortex *in vitro*. We then determined the number and placement of the corresponding interaction sites by high-resolution electron microscopy. We also measured the efficacy of various types of intercellular interactions by which presynaptically evoked gamma-frequency firing could set the phase of postsynaptic action potentials.

Results

The first class of interneuron–interneuron connections was mediated by chemical synapses only ($n = 12$). Inhibitory postsynaptic potentials (IPSPs) showed paired pulse depression (paired pulse ratio = 0.79 ± 0.14) and were mediated by $GABA_A$ receptors, as they could be completely abolished by bicuculline (20 μM; $n = 4$; **Fig. 1a–c**). Decay time constants of the inhibitory postsynaptic currents (IPSCs) were, on average, 8.33 ± 2.09 ms ($n = 8$). Presynaptic firing at gamma frequency resulted in the summation of postsynaptic unitary IPSPs and their use-dependent depression in all connections ($n = 4$). Initially, IPSP summation led to a modest increase in amplitude of the compound IPSP, which exceeded the amplitude of averaged single events by 30.1 ± 10.0%. Subsequently, responses gradually decreased to a relatively stable level at ~36 ± 8% of the summed peak response (**Fig. 1d**). Presynaptic spike trains (37 Hz) decreased the mean frequency of spontaneous postsynaptic firing to 59 ± 14% of the control value (from 3.94 ± 0.95 Hz to 2.33 ± 0.43 Hz), with most of the first postsynaptic action potentials occurring ~150 ms after onset of gamma-frequency presynaptic activity (**Fig. 1d**). Interestingly, all postsynaptic cells continued to discharge mainly at theta frequency following the cessation of presynaptic firing (**Fig. 1e**). Accordingly, peaks of spike-probability distributions indicated a clear phasing of postsynaptic activity in the theta frequency range (7.3 ± 2.1 Hz; not shown), with no apparent effi-

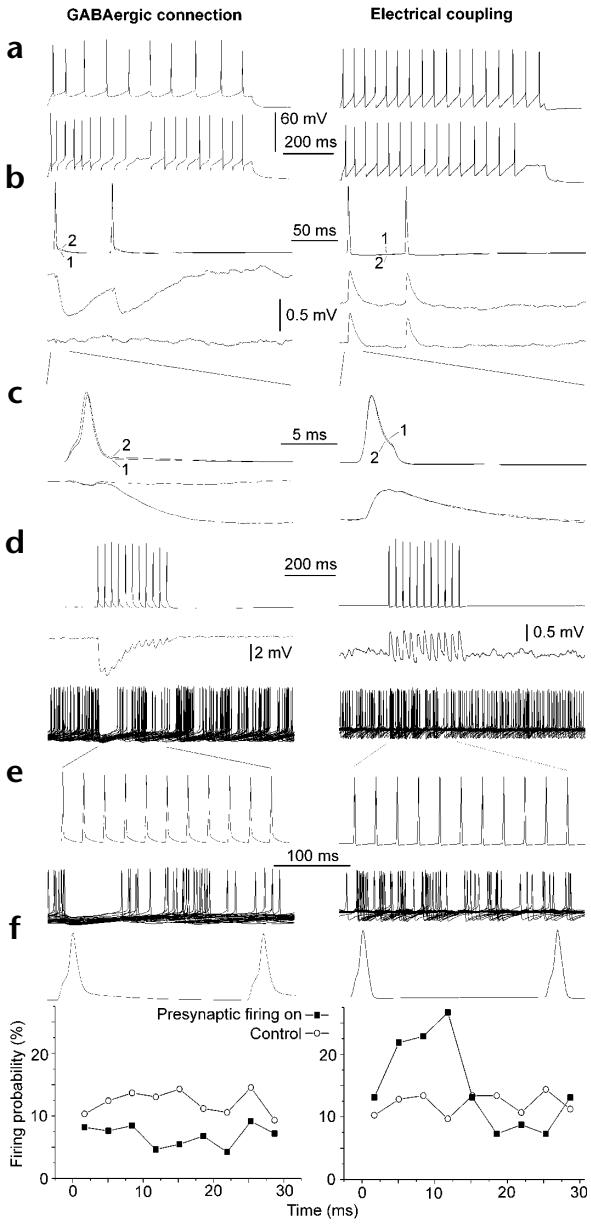

Fig. 1. Differential modulation of postsynaptic firing by presynaptic gamma-frequency activity in two interneuron–interneuron connections. (**a**) Firing pattern of the presynaptic (top) and postsynaptic (bottom) cells evoked separately by depolarizing current pulses. (**b**, left) IPSPs evoked in the postsynaptic cell by the presynaptic cell showed paired-pulse depression (middle); bicuculline (20 μM) antagonized the response (bottom). (**b**, right) In electrically coupled neurons, presynaptic action potentials elicited spikelets in the postsynaptic cell (middle), which remained unchanged in NBQX (20 μM), D-AP-5 (50 μM) and bicuculline (20 μM, bottom). (**c**) Expanded traces. (**c**, left) Rise of IPSP. (**c**, right) Onset of spikelets during the rising phase of the presynaptic spike. Action potentials during control (1) and drug application (2) superimpose perfectly. (**d**, left) Presynaptic cell firing at 37 Hz elicited IPSPs showing marked activity-dependent depression (middle). Subsequently, the postsynaptic cell was tonically depolarized to fire at ~5 Hz (bottom, 30 consecutive superimposed sweeps). (**d**, right) In the electrically coupled neurons, presynaptic firing elicited spikelets of stable amplitude (middle). On average, spike frequency in the postsynaptic cell increased to 121% of control (bottom). (**e**) Expanding the time scale shows that gamma-frequency IPSPs (left) phased firing with a considerable delay. Likewise, in the electrical connection (right) pre- and postsynaptic activity remained asynchronous, although the postsynaptic cell became effectively entrained with a short phase-lag. (**f**) Plots of firing probability for the postsynaptic cells during a representative presynaptic spiking cycle show that the two types of connections differ in their ability to phase postsynaptic activity at gamma frequency.

cacy at shorter intervals in the gamma frequency range (**Fig. 1f**). Comparable results were obtained from two interneuron-to-pyramidal cell connections (data not shown). The presynaptic GABAergic interneurons, which were tested in the gamma-frequency synchronization protocol ($n = 6$) were subsequently investigated by electron microscopy to establish their postsynaptic efferent target profile. All cells were identified as basket cells, forming synapses ($n = 67$) mainly on somata (32 ± 5%) or dendritic shafts (58 ± 6%) and, occasionally, on dendritic spines (10 ± 7%)[30,31]. Postsynaptic interneurons represented a heterogeneous population, as they responded to depolarizing current injections with a variety of firing patterns such as fast or regular spiking and showed heterogeneous light microscopic features.

The second class of interneuron–interneuron connections was mediated exclusively by electrical synapses ($n = 14$). Light microscopic analysis of all four fully visualized cell pairs indicated close appositions between either proximal dendrites or somata and dendrites, with one to four predicted contact sites. Electron microscopic analysis of the suspected sites was carried out in two cell pairs and yielded the identification of one gap junction in each connection; thus the site of electrical coupling between interneurons was unequivocally defined. A single gap junction mediated the first connection between proximal dendrites (**Fig. 2g–i**); the second interaction involved a dendrosomatic gap junction. Based on their postsynaptic target preference, interneurons of the fully recovered pairs ($n = 8$) could be classified as basket cells forming synapses ($n = 89$) predominantly on somata (31 ± 5%) and dendritic shafts (62 ± 10%) and, occasionally, on dendritic spines (7 ± 6%).

Gap junctional potentials (GJPs; $n = 14$) were of modest amplitude (0.52 ± 0.30 mV) at –55 ± 1 mV membrane potential and had an average duration of 5.92 ± 2.90 ms as measured at half amplitude. They followed presynaptic action potentials with a delay of 0.32 ± 0.12 ms, measured as the period spanning the maximal rates of rise of the presynaptic action potential and the GJP, respectively. Both amplitudes and kinetics of GJPs remained unchanged during repetitive presynaptic firing. The average amplitude ratio (coupling coefficient) of GJPs and presynaptic action potentials was 0.48 ± 0.14%. In view of the probable attenuation of GJPs due to the fast kinetics, amplitude ratios were also determined with current steps in the first neuron (200 pA, 300 ms duration), which were of sufficient duration for the response in the second neuron to reach a plateau. Indeed, when measured using long presynaptic current steps, the coupling ratio was found to be considerably larger (3.88 ± 0.68%; $n = 3$). Nevertheless, the coupling ratio of basket cells in layers 2/3 seemed to be half of that of fast-spiking cells in layers 4/5 (refs. 21, 22). The average gap junctional conductance was determined to be 334 ± 86 pS ($n = 4$), using voltage commands (± 20 mV; 300 ms) in the first neuron and measuring the current elicited in the second cell in voltage clamp mode. When tested ($n = 11$), unitary GJPs elicited by presynaptic spike trains at 37 Hz were either ineffective in modulating postsynaptic firing ($n = 6$) or entrained postsynaptic suprathreshold activity with a substantial phase lag ($n = 5$). In the latter cases, postsynaptic firing probability peaked 10.8 ± 2.8 ms

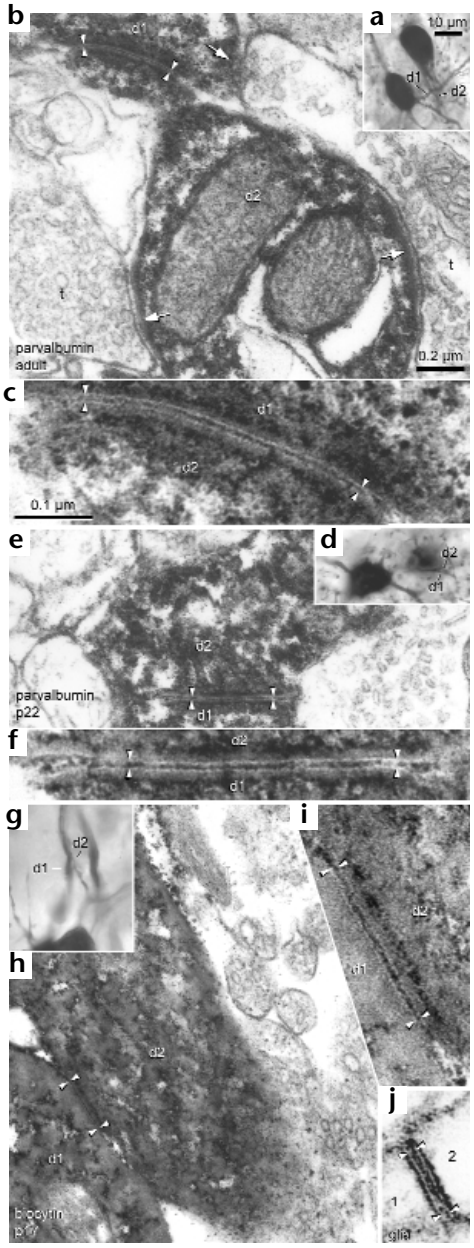

Fig. 2. Electron microscopic evidence for gap junctions between cortical interneurons. Light micrographs of parvalbumin-immunoreactive (**a**, **d**) and biocytin-filled (**g**) neurons taken from adult and young (22- and 17-day old; P22, P17) animals. The corresponding electron microscopic images (**b**, **e**, **h**) provide evidence that proximal dendrites (d1, d2) established gap junctions (between paired arrowheads). Synaptic junctions (arrows in **b**) targeting the same dendrites are indicated for comparison. (**c**, **f**, **h**) The electron-lucent stripe of membranes forming the gap junctions between interneurons containing peroxidase reaction end-product is equidistant to that of gap junctions between glial cells (1, 2) shown in panel (**j**).

after the preceding presynaptic spike. To assess putative activity-dependent changes on the likelihood of postsynaptic action potentials, firing-probability distributions were obtained for the first and subsequent five cycles, respectively. Statistical comparison showed no significant differences for those connections which were mediated by GJPs only (Friedman's test, $p > 0.05$). Electrical connections, which were effective in the entrainment of firing, increased the mean postsynaptic discharge rate from 3.93 ± 0.97 Hz to 4.87 ± 1.70 Hz (120 ± 13%). Because the postsynaptic cell fired tonically, the effect of such a modest increase in firing rate was unlikely to significantly shift the activation level of voltage and/or calcium-dependent conductances to introduce confounding factors beyond those due to the effects of GJPs.

The third class of unitary interneuronal connections ($n = 4$) was conjointly mediated by electrical and GABAergic interactions (**Figs. 3** and **4**). In two instances, coupled pairs of neurons were characterized by combining biocytin labeling with immunocytochemistry. All four cells were immunoreactive for parvalbumin (PV, **Fig. 4c**). Subsequently, all anatomically recovered interneurons ($n = 6$) in this group were electron microscopically identified as basket cells ($n = 82$ synapses), targeting predominantly somata (37 ± 7%) and dendritic shafts (57 ±12%), and, on occasion, dendritic spines (6 ± 6%). Detailed analysis of electron microscopy of two connections revealed gap junctions as well as chemical synapses within the perisomatic domain of the postsynaptic cells. In the first pair of cells, two dendrosomatic gap junctions and three GABAergic synapses could be verified on the soma, with an additional synapse on a proximal dendrite (**Fig. 4b**). The interaction between the second pair of cells was mediated by a proximal dendrodendritic gap junction and a GABAergic synapse at a distance of 2.5 µm, by 2 additional axodendritic and 2 axosomatic synapses. When measured along the plasma membrane, the average distance between electrical and chemical synapses in the 2 connections was estimated to be 13.7 ± 11.2 µm. Moreover, all interaction sites were located in the perisomatic domain; mean distance of gap junctions from the soma was 3.6 ± 6.2 µm, and GABAergic synapses were positioned slightly farther, at 9.1 ± 12.3 µm.

Postsynaptic responses were composed of GJPs followed by short-latency IPSPs mediated by $GABA_A$ receptors and showing paired-pulse depression (paired-pulse ratio, 0.62 ± 0.17; **Fig. 3b**). IPSPs dramatically curtailed the decay of GJPs, as the subsequent application of bicuculline resulted in a more than 3-fold increase in the half-width of GJPs from 1.4 ± 0.5 ms to 4.8 ± 1.0 ms ($n = 4$; **Fig. 3c**). As in purely $GABA_A$ receptor-mediated connections, a marked use-dependent depression of IPSPs could be observed, with composite responses gradually approaching a relatively stationary level of ~34 ± 10% of the first event (**Fig. 3d**). Likewise, presynaptic spike trains at 37 Hz decreased the mean frequency of spontaneous postsynaptic firing to 74 ± 11% of control values (from 5.08 ± 1.19 Hz to 3.77 ± 1.13 Hz). However, following the onset of presynaptic spike trains postsynaptic firing was instantly synchronized, with no apparent phase-lag (bin width, 3.375 ms; **Fig. 3e–f**) and a relatively narrow temporal dispersion of action potentials. The initial precision of action potential timing was due primarily to $GABA_A$ receptor activation, and it decreased in parallel with the use-dependent depression of IPSPs (**Fig. 3e**). Consequently, maximal firing probability gradually shifted in phase by 3.4–6.8 ms (3 of 4 cases, not shown). Moreover, bicuculline either abolished the phasing of postsynaptic activity altogether ($n = 2$) or resulted in the development of a prominent phase-lag (~10 ms; $n = 2$; not shown).

The efficacy of presynaptic firing in phasing the postsynaptic cell clearly differed depending on the presence or absence of electrical and/or GABAergic coupling between individual pairs of cells. We tested whether the grouping of the cells according to the nature of their interaction would be similar to categories based solely on the postsynaptic firing behavior. Cluster analy-

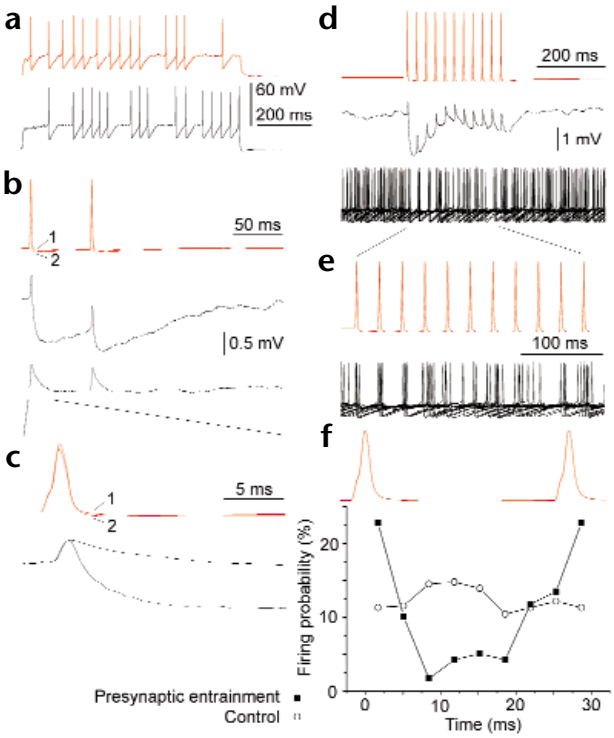

Fig. 3. A single presynaptic GABAergic neuron can synchronize postsynaptic firing at gamma-frequency by conjoint action of neighboring gap junctions and chemical synapses (**Fig. 4**). (**a**) Independently evoked firing patterns of the presynaptic (red) and postsynaptic (black) basket cell. (**b**) Presynaptic action potentials elicited spikelets followed by short-latency IPSPs in the coupled neuron. The IPSP showed paired-pulse depression (middle). Bicuculline (20 μM) blocked the hyperpolarizing, but not the depolarizing component of the response (bottom). (**c**) An expanded time scale shows that the GABAergic component starts at the peak of the spikelet, dramatically curtailing its decay, apparent in the presence of bicuculline. Upper traces show superimposed action potentials in control solution (1) and in bicuculline (2). (**d**) Presynaptic action potentials at 37 Hz elicited a compound response, consisting of spikelets of stable amplitude and decrementing IPSPs, leveling at a plateau of ~31% of the peak amplitude of the first event (middle). During presynaptic activity the average frequency of postsynaptic firing was reduced by 27% and, in contrast to purely electrical or synaptic connections, postsynaptic firing was effectively synchronized to presynaptic activity, also shown at an expanded time scale (**e**). (**f**) Temporal correlation of postsynaptic firing probability and a representative presynaptic action potential cycle.

sis of postsynaptic firing probability in response to gamma-frequency presynaptic interneuron firing resulted in the delineation of four categories of cells (**Fig. 5**). These groups generally corresponded to those delineated on the basis of the nature of synaptic interaction; however, cell pairs coupled only electrically fell into two groups according to the strength of coupling. Non-pyramidal cells form gap junctions in the adult hippocampus[25] and neocortex[23,24], but the incidence of dye coupling and gap junctions is affected by developmental changes[32,33]. Because our recordings were carried out in juvenile animals (P16–P20), we tested whether gap junctions, the anatomical substrate of electrical connections, are also present between parvalbumin-positive cells in adult animals. We observed evidence for gap junctions between PV-immunoreactive cells in both young (P22) and adult perfusion-fixed animals (**Fig. 2**). Gap junctions could be identified between the proximal dendrites and/or somata of all selected juxtaposed PV-positive cell pairs (P22, $n = 4$ pairs; adult, $n = 5$ pairs).

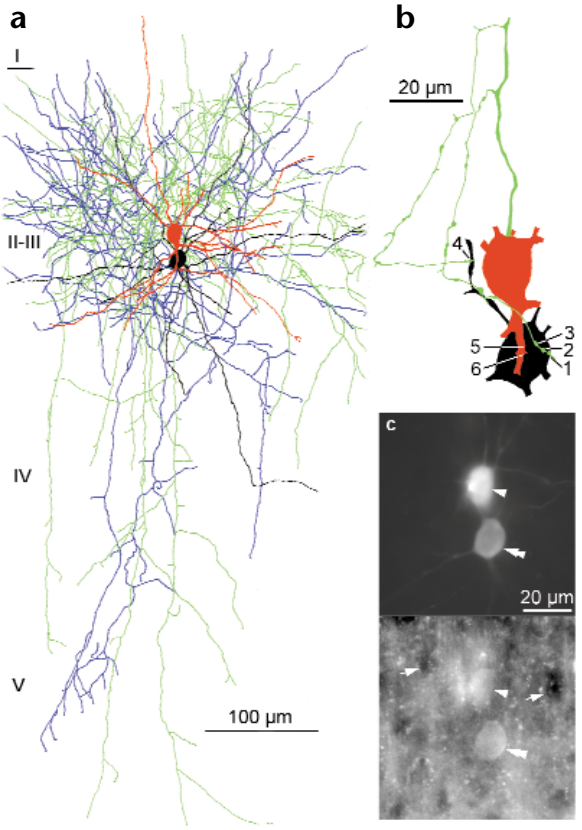

Discussion

Our results suggest that within interneuronal networks, electrical and synaptic coupling act synergistically to enhance the degree and precision of neuronal synchronization. The relative timing of GJPs and IPSPs originating in the same presynaptic cell is invariant, thereby generating a precisely molded, biphasic postsynaptic compound potential which efficiently dictates the timing of postsynaptic action potentials. In addition, electron microscopy reveals that the spatial proximity of the interaction is bound to accentuate phasing accuracy by allowing local integration of GJPs and IPSPs. The proximal placement of synapses on or close to the soma minimizes the effects of dendritic filtering and the time required for signal propagation.

Fig. 4. Identification of interneurons involved in conjoint electrical and synaptic interaction as shown in Fig. 3. (**a**) Reconstructions of the presynaptic (soma and dendrites, red; axon, green) and postsynaptic (soma, dendrites: black, axon: blue) cells. Cortical layers (I–V) are indicated on the left. (**b**) The electron-microscopically identified synaptic junctions (1–4) and gap junctions (5, 6) mediating the interaction between the coupled cells were found nearby on the soma and a proximal dendrite. (**c**) Both presynaptic (arrowhead) and postsynaptic (double arrowhead) cells were parvalbumin-immunoreactive, as shown by the corresponding light micrographs (top, AMCA-streptavidin for biocytin; bottom, FITC imunofluorecence for parvalbumin). Arrows indicate parvalbumin-immunonegative somata.

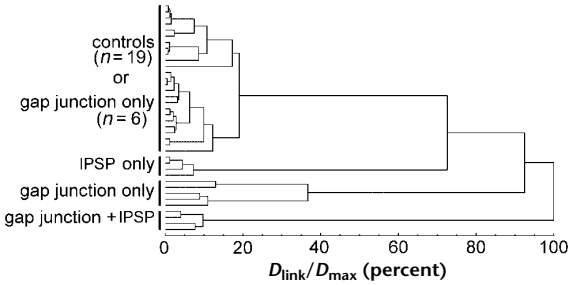

Fig. 5. Classification of postsynaptic interneuron firing behavior by cluster analysis of firing probability in response to gamma-frequency presynaptic firing. The firing behaviors fall into four groups. The first cluster contains all controls (absence of presynaptic firing, n = 16) and 6 connections mediated only by gap junctions, ineffective in altering postsynaptic firing. The second cluster comprises connections mediated by $GABA_A$ receptor-mediated IPSPs. Electrical connections that phase-lock but do not synchronize postsynaptic firing to the presynaptic cell is also a distinct group; interactions mediated by gap junctions as well as $GABA_A$ receptor-mediated synaptic responses comprise an additional group. Differences between clusters were significant in all permutations ($p \leq 0.03$–0.001; Friedman's test). D_{link}/D_{max}, linking and maximal Euclidean distances.

Both electrical and chemical synapses are reported between striatal[20], hippocampal[25] and neocortical[21,22] GABAergic neurons. Therefore, the synergy of mixed electrical and GABAergic coupling might represent a general mechanism for the synchronization of neural population activity in a variety of CNS regions. Here we identified electrically coupled cells as parvalbumin-expressing basket cells by assessing the quantitative distribution of their postsynaptic targets. Basket cells also target their own perisomatic domain via autapses[34]. Therefore, following an action potential and the activation of autaptic receptors, gap junctional re-excitability by the electrically coupled partners in the network might be limited.

The precise coupling of electrical and synaptic interactions affects the degree of synchrony, whereas the frequency of oscillations in inhibitory neuronal networks is probably a function of the decay time constants of the inhibitory postsynaptic currents (IPSCs)[10,14–16]. The average time constant of 8.3 ms measured in the connections presented here is compatible with experimental measurements and theoretical predictions as a determining factor for gamma-frequency oscillatory activity[10].

Mutual electrical connections between fast spiking (FS) cells or low-threshold spiking (LTS) cells seemed stronger in layers 4 and 5 than in layers 2/3 of the somatosensory cortex. Indeed, electrical coupling alone can synchronize pairs of interneurons[21,22]. Because FS and LTS cells are activated differently by thalamocortical input[21], strong electrical coupling of the same types of cells would favor a functional segregation of the two differentially connected interneuron networks, thereby providing two segregated streams of inputs to principal cells. In contrast, we show that, depending on the nature of their synaptic inputs, postsynaptic cells in layers 2/3 may differentially transform gamma-frequency activity of presynaptic basket cells.

On their own, gamma-frequency IPSPs elicited by basket cells could set the phase of activity of postsynaptic neurons in the theta frequency range. In those interactions mediated solely by GABAergic synapses, the latency of the postinhibitory delay of firing seemed to be determined by the time course of use-dependent IPSP depression, during persistent gamma frequency presynaptic cell firing. The onset of postsynaptic firing after about 150 ms predisposes the cell to entrainment in the theta frequency range, presumably in interaction with intrinsic membrane potential oscillation as described for hippocampal pyramidal cells[9]. However, in experiments with pyramidal cells, a presynaptic interneuron fires only one or a brief burst of action potentials and the rebound firing is determined conjointly by the frequency of intrinsic subthreshold membrane oscillations and the decay kinetics of the IPSP, instead of its use-dependent suppression. Regardless of the underlying mechanism, such theta-frequency phasing might be broadly distributed in the cortex, given that basket cell outputs are widely divergent, innervating principal cells as well as several different types of interneuron[28].

Phasing at gamma frequency is achieved when, in addition to the chemical synapses, electrical synapses are also involved in transmitting information from basket cells to their postsynaptic targets. The precision of gamma-frequency entrainment is probably influenced by a number of factors, among them emergent properties of the network, the strength of electrical connections[21,22] and, as shown above, the combination of GABAergic and gap junctional coupling. We showed that in supragranular layers, where intracortical interactions dominate neuronal activity, gap junctional coupling is less efficient for the synchronization of interneuronal firing. In the absence of network activity, synchrony is achieved only by the postsynaptic integration of precisely timed GJPs and IPSPs. Both the amplitude and the duration of the GABAergic component of the compound potential reported here are amenable to activity-dependent changes and modulatory influences by endogenous substances and drugs. These factors may influence neuronal synchronization in an activity-dependent manner.

Methods

Electrophysiology. Young (P16–P20) Wistar rats were anesthetized by i.p. injection of ketamine (30 mg per kg) and xylazine (10 mg per kg), and coronal slices (350 μm) were prepared from their somatosensory cortices. Slices were incubated at room temperature for 1 h in a solution composed of 130 mM $NaCl_2$, 3.5 mM KCl, 1 mM NaH_2PO_4, 24 mM $NaHCO_3$, 1 mM CaCl, 3 mM $MgSO_4$, 10 D(+)-glucose, saturated with 95% O_2 and 5% CO_2. The solution used during recordings differed only in that it contained 3 mM $CaCl_2$ and 1.5 mM $MgSO_4$. Whole-cell patch-clamp recordings were obtained at ~32°C from concomitantly recorded pairs of layer II/II putative interneurons visualized by infrared DIC (differential interference contrast) videomicrospcopy (Zeiss Axioskop microscope, Hamamatsu CCD camera, Luigs & Neumann Infrapatch set-up and HEKA EPC 9/double patch-clamp amplifier). Micropipets (5–7 MΩ) were filled with 126 mM K-gluconate, 4 mM KCl, 4 mM ATP-Mg, 0.3 mM GTP-Na, 10 mM HEPES, 10 mM creatine phosphate and 8 mM biocytin at pH 7.25 and 300 mOsm. Signals were filtered at 5 kHz, digitized at 10 kHz and analyzed with PULSE software (HEKA). Presynaptic cells were stimulated with brief (2-ms) suprathreshold pulses at 60-ms intervals (16.6 Hz) for the paired-pulse protocol and at 37 Hz for the gamma-frequency phasing protocol. Depression of IPSPs fully develops only after four or more postsynaptic events, therefore we used ten presynaptic cycles to test the effect of the use-dependent suppression of IPSPs on the phasing of postsynaptic activity. We applied the same protocol throughout the study for consistency. To minimize intertrial variability, trains were delivered at intervals greater than five seconds. During paired-pulse trials, membrane potentials of postsynaptic cells were held at –55 ± 3 mV. For phasing trials, they were depolarized with constant current injections to just above threshold to elicit firing. Unless specified, traces shown are averages of 50–200 episodes. The amplitude of a postsynaptic event was defined as the difference between the peak amplitude and the baseline value measured before the IPSP onset. Firing-probability plots were constructed from 50–100 consecutive trials as follows: with-

in a given cycle (interval separating two presynaptic action potentials), postsynaptic spike latencies were measured from the peak of the preceding presynaptic action potential. Subsequently, unless otherwise specified, the data were pooled regardless of the position in the presynaptic spike train. Controls were collected before the onset of the presynaptic spike train using an identical cycle length. Data are given as mean ± s.d. Mann-Whitney *U*-tests were used for statistical analysis, differences were considered statistically significant if $p \leq 0.05$. Interneurons were classified by cluster analysis based on postsynaptic cell firing probability (Statistica for Windows, StatSoft, Tulsa, Oklahoma). Joining trees based on Euclidean distances were constructed by Ward's method of amalgamation[35]. Using the number of clusters given by this *a priori* cluster analysis, we also used *k*-means clustering on the data *a posteriori*. The latter method grouped the same connections into each particular cluster.

Histology. Visualization of biocytin for permanent preparations, light microscopic reconstructions and correlated light- and electron microscopy was performed as described earlier[30,31]. Monoclonal antibodies to parvalbumin (Sigma, diluted 1:500) and rabbit antibodies to the C-terminal nonapeptide (107–115) of rat pro-cholecystokinin (diluted 1:1000) were co-applied to characterize interneurons. Triple fluorescence immunolabeling of hippocampal slices containing recorded and biocytin-filled cells was carried out as described[29], using AMCA-conjugated streptavidin (Vector Labs, Burlingame, California) for revealing biocytin, Alexa488-conjugated anti-mouse IgG (Molecular Probes, Eugene, Oregon) for parvalbumin and CY3-conjugated anti-rabbit IgG (Jackson Labs, West Grove, Pennsylvania) for revealing CCK. None of the cells was immunopositive for CCK. Images were recorded digitally. For pre-embedding immunocytochemistry, a young (P22) and a 3-month old Wistar rat were deeply anaesthetized (sodium pentobarbital, 150 mg per kg, intraperitoneal) and perfused with a fixative containing 4% paraformaldehyde, 0.05% glutaraldehyde and 0.2% picric acid in 0.1 M phosphate buffer. Vibratome sections (60 μm) were incubated with the antibody to parvalbumin (as above) and then reacted with the avidin-biotinylated peroxidase complex (Vector Labs). Parvalbumin immunoreactivity was visualized with diaminobenzidine tetrahydrochloride.

Acknowledgements

We thank N. Kogo, G. Maccaferri and O. Paulsen for scientific advice and technical help and J. D. B. Roberts and P. Jays for technical assistance. This work was also supported by the James S. McDonnell Foundation (EESI grant No 97-39), the Wellcome Trust, a European Commission Shared Cost RTD Program (No. BIO4CT96-0585) and the Hungarian Scientific Research Fund. G. T. was a Zoltán Magyary and OTKA Scholar during part of this project.

Received 29 November 1999; accepted 17 February 2000

1. Niedermeyer, E. & Lopes da Silva, F. *Electroencephalography: Basic Principles, Clinical Applications and Related Fields* (Williams and Wilkins, Baltimore, 1993).
2. Jefferys, J. G. R., Traub, R. D. & Whittington, M. A. Neuronal networks for induced '40 Hz' rhythms. *Trends Neurosci.* **19**, 202–208 (1996).
3. Mainen, Z. F. & Sejnowski, T. J. Reliability of spike timing in neocortical neurons. *Science* **268**, 1503–1506 (1995).
4. Singer, W. & Gray, C. M. Visual feature integration and the temporal correlation hypothesis. *Annu. Rev. Neurosci.* **18**, 555–586 (1995).
5. Lisman, J. E. & Idiart, M. A. P. Storage of 7 +/– 2 short-term memories in oscillatory subcycles. *Science* **267**, 1512–1515 (1995).
6. Singer, W. Neuronal synchrony: a versatile code for the definition of relations? *Neuron* **24**, 49–65 (1999).
7. Buzsaki, G. & Chrobak, J. J. Temporal structure in spatially organized neuronal ensembles: a role for interneuronal networks. *Current Neurobiol.* **5**, 504–510 (1995).
8. Csicsvari, J., Hirase, H., Czurko, A., Mamiya, A. & Buzsaki, G. Oscillatory coupling of hippocampal pyramidal cells and interneurons in the behaving rat. *J. Neurosci.* **19**, 274–287 (1999).
9. Cobb, S. R., Buhl, E. H., Halasy, K., Paulsen, O. & Somogyi, P. Synchronization of neuronal activity in hippocampus by individual GABAergic interneurons. *Nature* **378**, 75–78 (1995).
10. Traub, R. D., Whittington, M. A., Stanford, I. M. & Jefferys, J. G. R. A mechanism for generation of long-range synchronous fast oscillations in the cortex. *Nature* **383**, 621–624 (1996).
11. Ylinen, A. *et al.* Intracellular correlates of hippocampal theta rhythm in identified pyramidal cells, granule cells, and basket cells. *Hippocampus* **5**, 78–90 (1995).
12. Lytton, W. W. & Sejnowski, T. J. Simulations of cortical pyramidal neurons synchronized by inhibitory interneurons. *J. Neurophysiol.* **66**, 1059–1079 (1991).
13. Swadlow, H. A., Beloozerova, I. N. & Sirota, M. G. Sharp, local synchrony among putative feed-forward inhibitory interneurons of rabbit somatosensory cortex. *J. Neurophysiol.* **79**, 567–582 (1998).
14. Buhl, E. H., Tamas, G. & Fisahn, A. Cholinergic activation and tonic excitation induce persistent gamma oscillations in mouse somatosensory cortex in vitro. *J. Physiol. (Lond.)* **513**, 117–126 (1998).
15. Fisahn, A., Pike, F. G., Buhl, E. H. & Paulsen, O. Cholinergic induction of network oscillations at 40 Hz in the hippocampus in vitro. *Nature* **394**, 186–189 (1998).
16. Whittington, M. A., Traub, R. D. & Jefferys, J. G. R. Synchronized oscillations in interneuron networks driven by metabotropic glutamate receptor activation. *Nature* **373**, 612–615 (1995).
17. Christie, M. J., Williams, J. T. & North, R. A. Electrical coupling synchronizes subthreshold activity in locus coeruleus neurons in vitro from neonatal rats. *J. Neurosci.* **9**, 3584–3589 (1989).
18. Mann-Metzer, P. & Yarom, Y. Electrotonic coupling interacts with intrinsic properties to generate synchronized activity in cerebellar networks of inhibitory interneurons. *J. Neurosci.* **19**, 3298–3306 (1999).
19. Draguhn, A., Traub, R. D., Schmitz, D. & Jefferys, J. G. Electrical coupling underlies high-frequency oscillations in the hippocampus in vitro. *Nature* **394**, 189–192 (1998).
20. Koos, T. & Tepper, J. M. Inhibitory control of neostriatal projection neurons by GABAergic interneurons. *Nat. Neurosci.* **2**, 467–472 (1999).
21. Gibson, J. F., Beierlein, M. & Connors, B. W. Two networks of electrically coupled inhibitory neurons in neocortex. *Nature* **402**, 75–79 (1999).
22. Galarreta, M. & Hestrin, S. A network of fast-spiking cells in the neocortex connected by electrical synapses. *Nature* **402**, 72–75 (1999).
23. Sloper, J. J. Gap junctions between dendrites in the primate neocortex. *Brain. Res.* **44**, 641–646 (1972).
24. Peters, A. Morphological correlates of epilepsy: cells in the cerebral cortex. *Adv. Neurol.* **27**, 21–48 (1980).
25. Kosaka, T. & Hama, K. Gap junctions between non-pyramidal cell dendrites in the rat hippocampus (CA1 and CA3 regions): a combined Golgi-electron microscopy study. *J. Comp. Neurol.* **231**, 150–161 (1985).
26. Pappas, G. D. & Bennett, M. V. Specialized junctions involved in electrical transmission between neurons. *Ann. NY Acad. Sci.* **137**, 495–508 (1966).
27. Nakajima, Y. Fine structure of the synaptic endings on the Mauthner cell of the goldfish. *J. Comp. Neurol.* **156**, 375–402 (1974).
28. Tamas, G., Somogyi, P. & Buhl, E. H. Differentially interconnected networks of GABAergic interneurons in the visual cortex of the cat. *J. Neurosci.* **18**, 4255–4270 (1998).
29. Reyes, A. *et al.* Target-cell-specific facilitation and depression in neocortical circuits. *Nat. Neurosci.* **1**, 279–285 (1998).
30. Tamas, G., Buhl, E. H. & Somogyi, P. Fast IPSPs elicited via multiple synaptic release sites by distinct types of GABAergic neuron in the cat visual cortex. *J. Physiol. (Lond.)* **500**, 715–738 (1997).
31. Buhl, E. H., Halasy, K. & Somogyi, P. Diverse sources of hippocampal unitary inhibitory postsynaptic potentials and the number of synaptic release sites. *Nature* **368**, 823–828 (1994).
32. Peinado, A., Yuste, R. & Katz, L. C. Extensive dye coupling between rat neocortical neurons during the period of circuit formation. *Neuron* **10**, 103–114 (1993).
33. Connors, B. W., Benardo, L. S. & Prince, D. A. Coupling between neurons of the developing rat neocortex. *J. Neurosci.* **3**, 773–782 (1983).
34. Tamas, G., Buhl, E. H. & Somogyi, P. Massive autaptic self-innervation of GABAergic neurons in cat visual cortex. *J. Neurosci.* **17**, 6352–6364 (1997).
35. Ward, J. H. Hierarchical grouping to optimize an objective function. *J. Am. Stat. Assoc.* **58**, 236 (1963).